














Laser-induced demagnetization in van der Waals XY - and Ising-like antiferromagnets $NiPS_3$ and $FePS_3$

D. V. Kuntu ^{1,*}, E. A. Arkhipova ¹, L. A. Shelukhin ¹, F. Mertens ², M. A. Prosnikov ¹, I. A. Eliseyev ¹,
A. N. Smirnov ¹, V. Yu. Davydov ¹, S. Mañas-Valero ³, E. Coronado ³, M. Cinchetti ² and A. M. Kalashnikova ¹

¹*Ioffe Institute, 194021 St. Petersburg, Russia*

²*Department of Physics, TU Dortmund University, Otto-Hahn-Straße 4, Dortmund 44227, Germany*

³*Instituto de Ciencia Molecular (ICMol), Universidad de Valencia, Paterna 46980, Spain*

 (Received 11 July 2023; revised 20 November 2023; accepted 15 December 2023; published 26 January 2024)

The critical behavior of laser-induced changes in magnetic ordering is studied experimentally in two-dimensional zigzag antiferromagnets XY -like $NiPS_3$ and Ising-like $FePS_3$. To examine laser-induced dynamics in flakes of these compounds, we employ time-resolved exchange linear dichroism effect sensitive to zigzag magnetic ordering and independent of the orientation of the antiferromagnetic vector. In both compounds laser excitation in the vicinity of the absorption edge induces partial quenching of the antiferromagnetic ordering manifested by exchange linear dichroism reduction. The amplitude of the effect varies with temperature as the derivative of the antiferromagnetic vector and exhibits a critical behavior with the exponents corresponding to XY and Ising models for $NiPS_3$ and $FePS_3$, respectively. Critical slowing down of the demagnetization in the vicinity of Néel temperature is found, however, only in $FePS_3$. In contrast, the increase of the demagnetization time near the ordering temperature in $NiPS_3$ is minor. We show that the difference in the demagnetization times correlates well with the spin specific heat in both compounds. Beyond the range of slowing down, the demagnetization times in $NiPS_3$ and $FePS_3$ are comparable, about 5–10 ps, and are longer than those reported earlier for $CoPS_3$ and considerably shorter than for $MnPS_3$. This points to the importance of the unquenched angular momentum of transition-metal ions in laser-induced demagnetization process.

DOI: [10.1103/PhysRevMaterials.8.014408](https://doi.org/10.1103/PhysRevMaterials.8.014408)

I. INTRODUCTION

The phenomenon of ultrafast demagnetization, namely quenching of the magnetic ordering in magnets following excitation with femtosecond laser pulses, has become a challenging topic for experimental and theoretical studies. It yielded discoveries of single- and multishot all-optical magnetic reversal [1–3], generation of ultrashort spin currents [4], and emission of broadband THz pulses [5]. In metals, demagnetization is governed by electron-phonon coupling [6], leading to characteristic timescales of the process of less than 100 femtoseconds [7–9]. In insulators, this timescale is defined mainly by spin-lattice coupling, and the demagnetization process develops in a subnanosecond range [10,11]. The ultrafast demagnetization process is also intrinsically sensitive to critical phenomena occurring in the vicinity of magnetic ordering temperature [12,13]. Therefore, the type and dimensionality of the magnetic ordering can play an important role in this process, along with the electronic band structure and coupling of spins to other energy and angular momenta reservoirs.

Layered magnetic materials, such as van der Waals materials [14,15], organic-inorganic hybrids [16], MAX phases [17], etc., offer an appealing possibility to investigate ultrafast magnetic dynamics in connection to details of magnetic ordering. Indeed, while having similar crystallographic structure within

a family, these materials demonstrate a broad variety of spin arrangements. Another common feature of such compounds is a weak interlayer exchange coupling, making them quasi-two-dimensional (quasi-2D) structures. As a result, these materials are used for examining the Mermin-Wagner theorem and ways to overcome restrictions on magnetic ordering in the 2D limit [18]. In a few- and single-layer limit readily achievable for, e.g., van der Waals materials [19–22], their magnetic ordering can experience drastic changes such as a transition between different spin alignments [23] or quenching of magnetic ordering [24], although the latter remains a matter of further discussion [25].

Laser-pulse-driven spin dynamics in layered magnets has recently become a subject of active studies. They cover revealing manifestations of a quasi-2D nature of magnetic ordering [26], as well as examining coupling between lattice and spins and its effect on laser-driven processes in both subsystems [27–31]. Examination of a critical behavior of the laser-induced spin dynamics takes a central place in many of these studies [30–32], with van der Waals transition-metal thiophosphates MPS_3 ($M = Mn, Fe, Co, Ni$) playing an essential role as the materials offering a variety of antiferromagnetic (AFM) arrangements [14].

In this paper, we report on a comparative study of laser-induced demagnetization in the van der Waals transition-metal thiophosphates $NiPS_3$ and $FePS_3$. Within the MPS_3 family, nickel and iron phosphorus trisulfides possess a number of similarities with each other and are very distinct from the other two compounds. Namely, $FePS_3$ and $NiPS_3$

*dariya.kuntu@mail.ioffe.ru

both are zigzag antiferromagnets, and their magnetism is of predominantly spin origin. Yet, FePS₃ demonstrates the 2D Ising-like critical properties, while those of NiPS₃ are described by the 2D XY model. By studying the time-resolved dynamics of the exchange linear dichroism (exLD), we reveal that the demagnetization degree in both thiophosphates increases in the vicinity of the Néel temperature and is governed by the critical behavior of the order parameter depending on the type of 2D magnetic ordering. However, only 2D Ising-like antiferromagnet FePS₃ exhibits a pronounced slowing down of the demagnetization rate as Néel temperature is approached, while in 2D XY-like NiPS₃, such a slowing down in the vicinity of T_N is minor. Using a two-temperature model for the lattice and the spin responses to the optical excitation, we identify that the difference in demagnetization times stems from distinct spin heat capacity behaviors.

II. EXPERIMENTAL

A. Materials and samples characterization

NiPS₃ and FePS₃ from the family of transition-metal thiophosphates MPS_3 are layered van der Waals materials [14]. They belong to a monoclinic crystal system, space group $C2/m$ (#12) [33]. As shown in Figs. 1(a) and 1(b) the transition-metal ions are arranged in a honeycomb structure within the ab plane [34,35]. The band gap of NiPS₃ and FePS₃ is 1.7 eV and 1.5 eV, respectively [36], and is defined by the charge-transfer transitions involving states of P and S ions. Within a band gap there are weaker $d-d$ transitions of M^{2+} ions in the near-infrared range [37].

Among MPS_3 , nickel and iron thiophosphates have the most similarities in terms of spin arrangement. Furthermore, they take an intermediate place in terms of quenching the orbital momentum of a magnetic ion between MnPS₃ (the zero orbital momentum of Mn^{2+}) and CoPS₃ (the largest orbital momentum) [34]. Thus, they suit well for the comparative study of laser-induced demagnetization. The Néel temperatures are $T_N = 155$ K for NiPS₃ and $T_N = 118$ K for FePS₃ [34]. As illustrated in Fig. 1(a), in NiPS₃, magnetic moments form ferromagnetically (FM) coupled zigzag chains. The chains are AFM coupled within the ab plane and FM coupled in the adjacent layers along the c axis [35]. In samples with a thickness of more than 50 nm, the AFM vector \mathbf{L} lies along a axis with a small deviation from the ab plane [35,38]. This magnetic system can be described by the 2D XY or XXZ model [24]. In FePS₃, the zigzag ordering in the ab plane is the same, while the chains are AFM coupled in adjacent layers Fig. 1(b). In contrast to NiPS₃, the magnetic properties of FePS₃ are described by the 2D Ising model. \mathbf{L} is perpendicular to the layers [39]. The magnetic order is preserved at least down to the bilayer in NiPS₃ [24] and to the monolayer in FePS₃ [25,40].

Flakes of NiPS₃ and FePS₃ were obtained from the crystals grown by solid-state reaction, as detailed in Refs. [27,42]. They were mechanically exfoliated using adhesive tape inside an argon glove box, and deposited onto Si/285 nm SiO₂ substrates. Samples were characterized by atomic force microscopy, as shown in Figs. 1(c) and 1(d). The lateral sizes of NiPS₃ and FePS₃ flakes are ≈ 80 and ≈ 90 μm , respectively. Average flake thicknesses amounted to 200 nm and 180 nm,

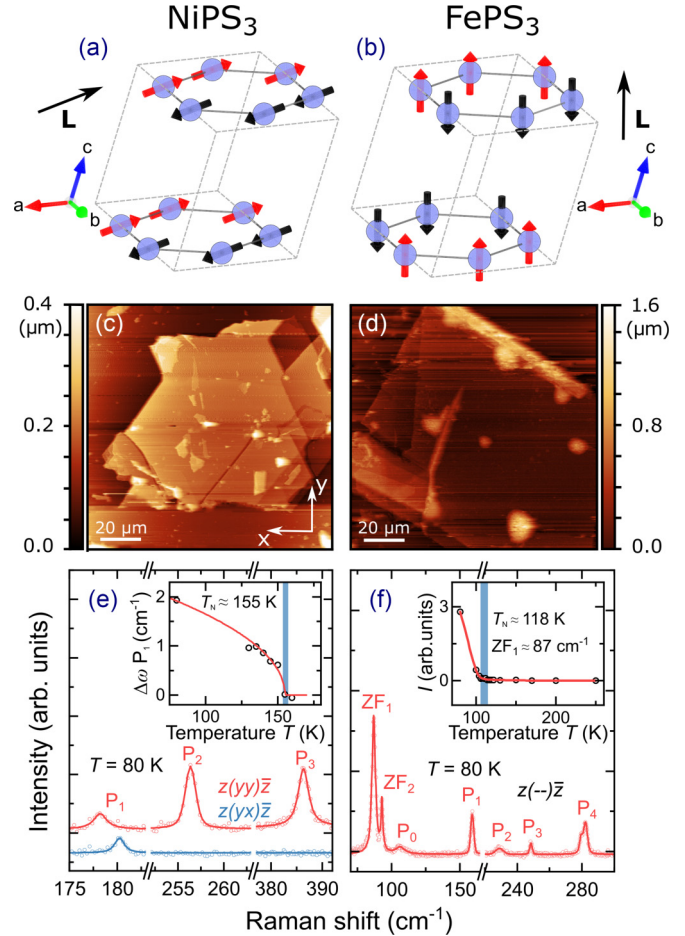


FIG. 1. (a), (b) Magnetic structure of (a) NiPS₃ and (b) FePS₃, blue spheres represent metal atoms. \mathbf{L} is the antiferromagnetic vector. The figure was created using the VESTA [41]. (c), (d) Atomic force microscopy images of (c) NiPS₃ and (d) FePS₃ flakes on Si/SiO₂ substrate. (e) Polarized Raman spectra of NiPS₃ measured at $T = 80$ K in parallel $[z(yy)\bar{z}]$ and crossed $[z(yx)\bar{z}]$ scattering configurations. Inset shows temperature dependence of magnetic-order-induced frequency difference $\Delta\omega$ for phonon lines P_1 in parallel and cross polarization configurations. The red line represents fit by the function $\propto |T - T_N|^{2\beta}$. (f) Nonpolarized Raman spectrum of FePS₃ measured at $T = 80$ K. Inset shows the integral intensity I of the low-frequency ZF_1 phonon peak (87 cm^{-1}) as a function of T . Red line is a guide for the eye. Blue vertical bars in (e), (f) mark T_N extracted from Raman lines temperature dependences.

respectively, i.e., their properties are expected to correspond to those of the bulk samples.

For a detailed characterization, Raman measurements were performed using a LabRAM HR Evolution UV-VIS-NIR (Horiba, France) spectrometer equipped with a confocal microscope. The spectra were measured using continuous-wave excitation at the 532 nm (2.33 eV) line of a Nd:YAG laser, and the power of the incident light on the sample was limited to 0.4 mW. The spectra were recorded using an 1800 lines/mm grating and a nitrogen-cooled charge-coupled device detector, while a Leica PL FLUOTAR 50 (NA = 0.55) long working-distance objective lens was used to focus the incident beam into a spot of 2 μm diameter. For both samples, the sets of phonon lines in the obtained spectra shown in

Figs. 1(e) and 1(f) are in good agreement with literature data [24,40,43]. The temperature dependence of the intensity and frequency of the selected lines is used to examine the transition to the AFM phase. In order to control the sample temperature, a Linkam THMS600 (Linkam Scientific Instruments, UK) temperature control system was used. Polarized Raman spectra of NiPS₃ were measured in parallel [$z(yy)\bar{z}$] and crossed [$z(yx)\bar{z}$] scattering configurations, with z being the normal of the flake and x being along its horizontal side, as shown in Fig. 1(c). Figure 1(e) shows the spectra obtained at $T = 80$ K. In the paramagnetic phase of NiPS₃, the phonon peak P₁ is observed at a frequency of 178.3 cm⁻¹ for both polarizations. In the AFM state, the spectral positions of P₁ in parallel and crossed polarizations do not coincide due to the splitting of degenerate E -like phonon modes, which dramatically increases upon magnetic ordering [24]. The difference $\Delta\omega$ of P₁ frequencies for two polarizations as a function of T is shown in the inset of Fig. 1(e). Following Ref. [24], the temperature dependence is well described by $\Delta\omega \propto |T - T_N|^{2\beta}$, with a critical exponent $\beta = 0.24 \pm 0.04$ and $T_N = 155 \pm 0.5$ K, confirming 2D XY ($\beta = 0.231$ [44]) ordering and bulk Néel temperature, respectively.

The nonpolarized Raman spectrum for FePS₃ at $T = 80$ K is shown in Fig. 1(f). In the paramagnetic phase, there is a broad asymmetric phonon peak at 98 cm⁻¹ [45]. Below T_N , two distinct peaks at 87 and 93 cm⁻¹ appear due to the zone-folding (ZF) effect caused by the spin ordering [40]. The intensity of the ZF₁ peak at 87 cm⁻¹ grows with the decrease of T below T_N . As one can see from the inset of Fig. 1(f), the integral intensity I of this peak drops to zero at $T_N = 118$ K, which indicates the transition of FePS₃ to the paramagnetic phase. The obtained T_N value is in good agreement with previous studies of bulk FePS₃ [40,45].

B. Pump-probe experiment

Ultrafast magnetization dynamics in NiPS₃ and FePS₃ were measured with the femtosecond magneto-optical pump-probe technique. The experimental scheme is shown in Fig. 2(a). Probe pulses with a duration of 170 fs and a photon energy $E_{pr} = 1.2$ eV were generated by the Yb:KGW regenerative amplifier PHAROS (Light Conversion, Lithuania) at a repetition rate of 5 kHz. Optical parametric amplifier ORPHEUS (Light Conversion, Lithuania) was used as a source of pump pulses with photon energy in a range $E_p = 1.63$ – 1.97 eV and duration $\sigma \approx 170$ fs. Pump pulses had a fluence of $F = 2.5$ mJ/cm² and an angle of incidence of about 5°. The pump spot diameter at a sample was about 35 μ m. Probe pulses with a fluence of 7 mJ/cm² were focused on a sample into a spot with diameter of 11 μ m at a normal incidence. The optical response was checked to be linear at the given probe pulse fluence, as discussed in Appendix. Both pump and probe spots were smaller than the lateral sizes of the flakes, and it was possible to focus on an area without visible defects. Although within the laser spots the flakes possess some degree of thickness inhomogeneity, the latter is not expected to affect the magnetic or optical properties because of the overall large thickness of the flakes and the penetration depth of the pump and probe pulses exceeding

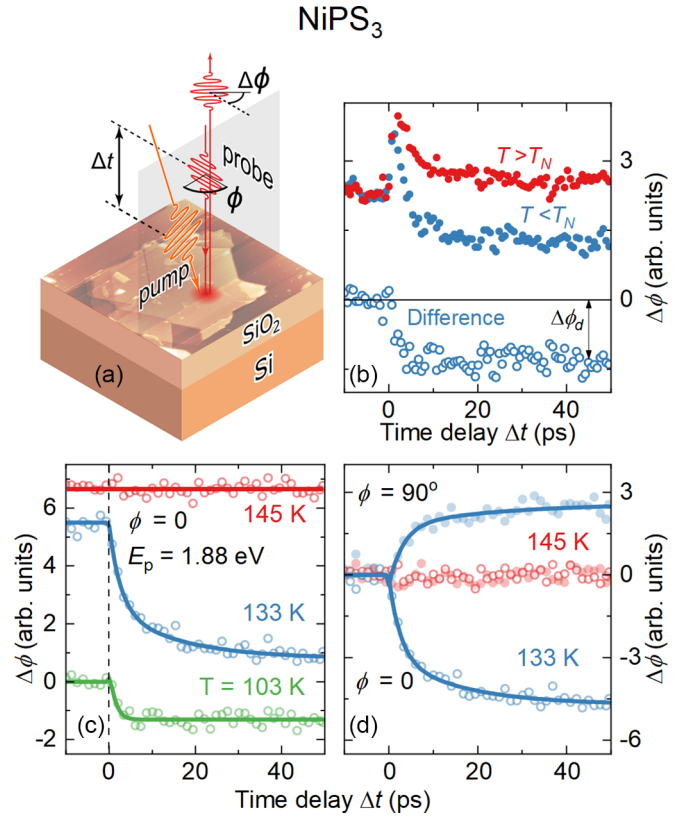


FIG. 2. (a) The time-resolved pump-probe experimental scheme. Gray shaded area depicts the plane of incidence for the pump pulses. Probe polarization angle ϕ is measured from this plane. (b) Laser-induced probe polarization rotation $\Delta\phi$ as a function of the delay time Δt measured in NiPS₃ flake at $T = 173$ K $> T_N$ (red solid symbols) and $T < T_N$ (blue solid symbols) and their difference (open blue symbols). $\Delta\phi_d$ at $\Delta t_d = 45$ ps is taken as an amplitude of the laser-induced change of exLD. (c) Laser-induced probe polarization rotation $\Delta\phi$ as a function of delay time Δt between pump ($E_p = 1.88$ eV) and probe pulses measured for different sample temperatures in NiPS₃. (d) Transient polarization rotation $\Delta\phi(\Delta t)$ measured at two probe linear polarizations $\phi = 0$ (open symbols) and $\phi = 90^\circ$ (solid symbols) at $T = 133$ K (blue symbols) and 145 K (red symbols). Solid lines are fit according to the Eq. (1).

it. They are found to be 300 nm and 4 μ m, respectively, for NiPS₃, and 800 nm and 7 μ m, respectively, for FePS₃.

The sample temperature was varied in the range $T = 78$ – 295 K with the temperature control system Linkam HFS600 (Linkam Scientific Instruments, UK). Pump-induced probe polarization $\Delta\phi$ and reflectivity ΔR were measured using balanced and single photodiode schemes, respectively, as functions of pump-probe time delay Δt . In Ref. [46], it was shown that AFM ordering in FePS₃ gives rise to an exLD, i.e., a difference in absorption and refraction for the light incident along the c axis and polarized along and perpendicularly to the zigzag chains, i.e., along the a and b axes, respectively. This effect stems from the sensitivity of the optical properties to the spin correlations and can also be seen as a magnetic refraction [47], which acquires anisotropy because of distinct exchange coupling along and perpendicular to chains. As a result, exLD gives rise to the rotation of the polarization of the reflected

light in the AFM phase. Since this effect is not sensitive to the orientation of \mathbf{L} , it is expected to be present in NiPS₃ and FePS₃ when the probe is incident along the flake normal. This is in contrast to quadratic magneto-optical Voigt and Kerr effects [48], which, in the considered geometry, require \mathbf{L} to lie in the sample plane and thus should vanish in the FePS₃ flake.

It was found that both $\Delta\phi(\Delta t)$ and $\Delta R(\Delta t)$ were temperature independent above T_N in both flakes (see Appendix, Fig. 5 for details). Thus, we used the pump-probe curves $\Delta\phi(\Delta t)$ measured at $T = 173$ K $> T_N$ for both compounds as reference data, which includes temperature-independent laser-induced optical response of the flakes, substrate, strain-induced dichroism, etc. Below, all presented data are the result of subtraction of the reference curve from a signal at a given temperature, as illustrated in Fig. 2(b) for the pump-induced rotation.

III. RESULTS

A. Laser-induced dynamics of exLD

The dynamics of the laser-induced probe polarization rotation in the NiPS₃ flake $\Delta\phi$ measured at different sample temperatures and probe polarizations is shown in Figs. 2(c) and 2(d). As seen in Fig. 2(c), below T_N there is a monotonic change of $\Delta\phi$ at $\Delta t > 0$, followed by a saturation. Relaxation to the initial state takes place at a longer time scale, which is inaccessible in our experiment. Noticeably, both the magnitude and characteristic time scale of $\Delta\phi(\Delta t)$ evolve with temperature, suggesting that the signal originates from the dynamics of magnetic properties. Furthermore, below T_N , $\Delta\phi(\Delta t)$ demonstrates pronounced dependence on the incident probe polarization angle ϕ , with the sign of the laser-induced changes reversed upon rotation of ϕ by 90° as shown in Fig. 2(d). The laser-induced changes of $\Delta\phi$ are absent for any ϕ above T_N . These temperature and probe polarization dependencies suggest that the measured signal is indeed the transient exLD, and, thus, represents the laser-driven evolution of the AFM ordering in NiPS₃.

The same measurements were performed for the FePS₃ flake [Fig. 4(c)], and yielded qualitatively similar trends, with clearly longer times characterizing the laser-induced change of exLD at some temperatures. In both samples, NiPS₃ and FePS₃, no dependence of $\Delta\phi(\Delta t)$ on pump polarization was observed in the whole studied temperature range. This points to the essential role of the ultrafast heating by a laser pulse in the measured dynamics.

Taking into account all the experimental observations, we conclude that in both NiPS₃ and FePS₃ below T_N the optical excitation causes the transient partial quenching of the AFM ordering, i.e., demagnetization, induced by the laser heating and manifesting itself via a decrease in exLD. We note that the laser-induced demagnetization in FePS₃ was earlier demonstrated in Ref. [32], while in NiPS₃ no data on this process at the picosecond timescale was reported.

Since the demagnetization is driven by ultrafast laser heating, it can be sensitive to the pump photon energy E_p due to the spectral dependence of the light absorption coefficient. To quantify the degree of demagnetization, we used the value

$\Delta\phi_d$ at $\Delta t_d = 45$ ps [Fig. 2(b)]. At most of the studied temperatures, the transient change of exLD saturates at this time delay in both NiPS₃ and FePS₃. The study of the laser-induced exLD dynamics in NiPS₃ as a function of the pump photon energy revealed that $\Delta\phi_d$ has a maximum at $E_p = 1.88$ eV [Fig. 3(b)]. This photon energy is in good agreement with the position of an absorption peak reported for NiPS₃ [49,50]. Based on this, we chose such a pump photon energy for measurements of temperature dependences in NiPS₃. In FePS₃, no pronounced spectral dependence of the signal was found, and the measurements were performed at $E_p = 1.97$ eV.

To analyze the temperature dependence of the laser-induced change of exLD and its features, we examined $\Delta\phi_d(T)$ and also found characteristic times by fitting experimental data at each temperature with a function

$$\Delta\phi(\Delta t, T) = \sum_{i=1}^2 B_i(T) [e^{-\Delta t/\tau_i(T)} - 1], \quad (1)$$

where B_i are the scaling parameters and τ_i are the time constants. Biexponential decay was introduced since in FePS₃ one clearly distinguishes faster (τ_1) and slower (τ_2) processes as shown in Fig. 4(c). The physical origin of the biexponential decay is discussed further. We note that the time delay $\Delta t_d = 45$ ps at which degree of demagnetization $\propto \Delta\phi_d$ is analyzed indeed exceeds $3\tau_2$ at most of the studied temperatures in NiPS₃ and FePS₃.

In NiPS₃, one can see that $\Delta\phi_d$ increases sharply with temperature and then abruptly decreases to zero [Fig. 3(a)]. This is, again, a characteristic behavior of the ultrafast laser-induced demagnetization, which is expected to be the largest

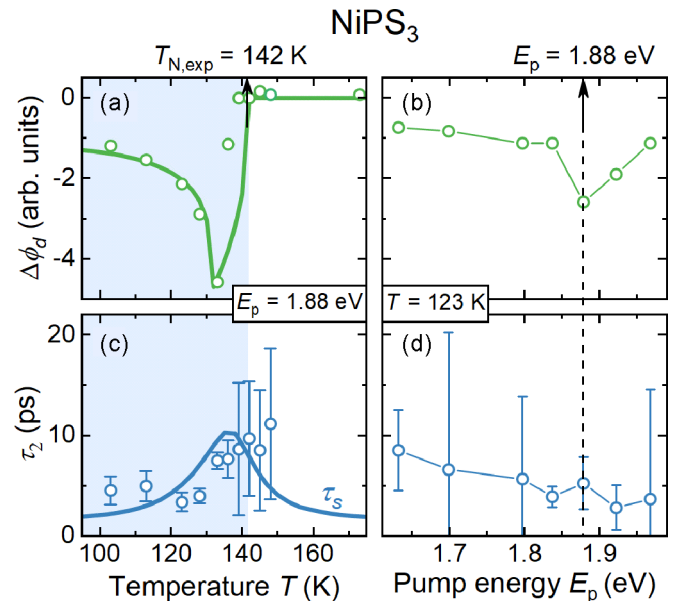


FIG. 3. (a), (b) Transient exLD amplitude $\Delta\phi_d$ and (c), (d) demagnetization time τ_2 in NiPS₃ as a function of (a), (c) sample temperature T with a fixed $E_p = 1.88$ eV and (b), (d) pump photon energy E_p with a fixed sample temperature $T = 123$ K. Incident probe polarization angle $\phi = 0$. Solid (a) green and (c) blue lines are fit according to Eqs. (3), (5) and Eqs. (4), (5), respectively.

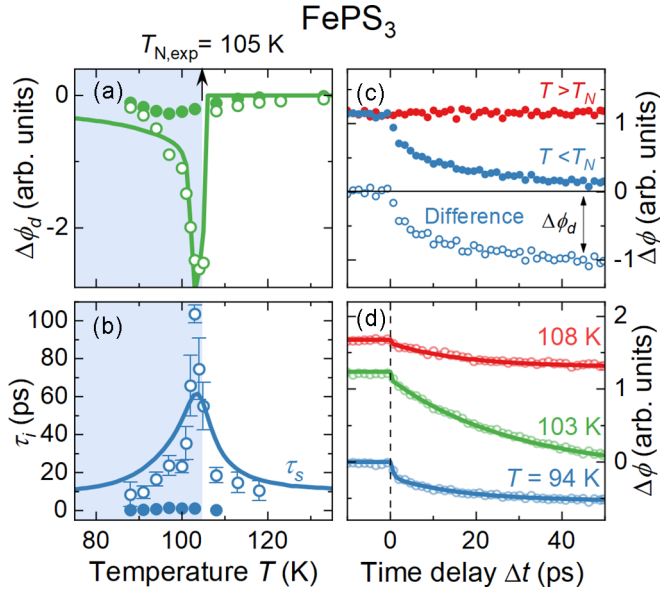


FIG. 4. (a) Transient exLD amplitude $\Delta\phi_d$ (open symbols) and (b) demagnetization time τ_2 (open symbols) in FePS₃ as a function of sample temperature with a fixed $E_p = 1.97$ eV. Also shown in (a), (b) are the amplitude $\Delta\phi(\Delta t = 2$ ps) and characteristic time τ_1 (solid symbols) of the optical contribution to $\Delta\phi$. (c) Laser-induced probe polarization rotation $\Delta\phi(\Delta t)$ measured in FePS₃ flake at $T = 173$ K $> T_N$ (red solid symbols) and $T = 94$ K $< T_N$ (blue solid symbols) and their difference (open blue symbols). (d) Transient polarization rotation $\Delta\phi$ measured in FePS₃ at different sample temperatures. Incident probe polarization angle $\phi = 0$. Solid (a) green and (b) blue lines are fit according to Eqs. (3), (5) and Eqs. (4), (5), respectively. Solid lines in (d) are fit according to Eq. (1).

just below T_N [10,11]. We ascribe the temperature at which the abrupt change of $\Delta\phi_d$ occurs to an experimental Néel temperature $T_{N,\text{exp}}$, which is below T_N determined from the Raman scattering study [see inset in Fig. 1(e)]. This is due to unideal thermal contact between the sample and the cold finger in the cryostat, as well as the excess laser heating not fully dissipating between the excitation events often present in the pump-probe experiments. The value of $T_{N,\text{exp}}$ is discussed below. The approximation of $\Delta\phi(\Delta t)$ using Eq. (1) gave $B_1 = 0$. Thus, τ_2 can be readily ascribed to a characteristic time of the AFM ordering decrease. τ_2 grows only slightly in the vicinity of $T_{N,\text{exp}}$ and does not exceed 15 ps in the whole studied range, as shown in Fig. 3(c).

Similarly, in FePS₃, a sharp increase of $\Delta\phi_d$ is observed as $T_{N,\text{exp}}$ is approached from below, followed by a sharp drop of the signal above it [Fig. 4(a)]. In contrast to NiPS₃, the approximation of $\Delta\phi(\Delta t)$ using Eq. (1) revealed the biexponential decay. The temperature dependencies of τ_1 and τ_2 are shown in Fig. 4(b). These time constants demonstrate distinct temperature dependences. τ_2 shows a pronounced increase up to 100 ps in the vicinity of $T_{N,\text{exp}}$, and we ascribe the temperature-dependent τ_2 to the demagnetization time [32], whereas $\tau_1 \approx 1.5$ ps is independent of T . Furthermore, the corresponding magnitude of the exLD change, $\Delta\phi(\Delta t = 2$ ps), gradually decreases as the temperature is swept across $T_{N,\text{exp}}$ towards the paramagnetic phase [Fig. 4(a)]. We note that the overall laser-induced polarization rotation $\Delta\phi(\Delta t)$ is

an order of magnitude larger in FePS₃ as compared to NiPS₃. Thus, the faster contribution to $\Delta\phi(\Delta t)$ in NiPS₃, if present, could be hindered by the sensitivity of the experimental technique.

Recently, fast demagnetization with a characteristic time of 1–5 ps was reported for another crystal from the MPS₃ family CoPS₃ [30]. It was suggested that the unquenched orbital momentum of Co²⁺ ions and strong spin-orbit coupling facilitate a faster demagnetization process in this compound. However, the degree and characteristic time of demagnetization in CoPS₃ demonstrated a pronounced increase near T_N . Thus, we can rule out such an origin of the fast contribution to $\Delta\phi(\Delta t)$ with τ_1 in FePS₃, although Fe²⁺ has unquenched orbital momentum as well. The demagnetization process with two faster and slower stages was also reported for a van der Waals ferromagnet Fe₃GeTe₂ [31]. In contrast to metallic Fe₃GeTe₂, spin-flip electron-phonon scattering responsible for the fast demagnetization [6] is negligible in nonmetallic FePS₃, and the two-stage demagnetization in FePS₃ can be ruled out.

To summarize the experimental findings, ultrafast demagnetization triggered by laser-induced heating is observed by means of the time-resolved exLD in both NiPS₃ and FePS₃. The demagnetization degree in both compounds possesses a sharp increase as the Néel temperature is approached. Demagnetization times, however, demonstrate distinct behavior, slowing down in the vicinity of the transition temperature found only in FePS₃. The underlying physical picture of the differences in the observed critical behavior of demagnetization dynamics in NiPS₃ and FePS₃ is discussed in the following section. In FePS₃, there is an additional faster process leading to changes in exLD with an origin distinct from that responsible for the demagnetization.

B. Numerical simulations of laser-induced dynamics of order parameter

ExLD scales as a squared order parameter L with temperature [46,51]. According to the Landau phase transition theory [52], the order parameter near T_N varies with temperature following the power law:

$$L \propto (T_N - T)^\beta, T < T_N$$

$$L = 0, T \geq T_N, \quad (2)$$

where β is the critical exponent. It characterizes the magnetic phase transition and is specific to a model describing the system. Consequently, an exact expression for the laser-induced change of exLD $\Delta\phi_d$ can be written as

$$\Delta\phi_d(T) = D(L^2 - L_0^2)$$

$$= D[(T_N - (T + \Delta T_s))^{2\beta} - (T_N - T)^{2\beta}], \quad (3)$$

where ΔT_s is the laser-induced change of the effective spin temperature and D is the scaling coefficient. In order to show a relation between the dynamics of laser-induced heating of the spin subsystem and $\Delta\phi_d(T, \Delta t)$ explicitly and to separate an effect of the critical behavior described by β from the effect of the spin temperature increase, we introduce the linear approximation of Eq. (3). The latter is valid under the assumption of relatively small laser-induced changes of L ,

i.e., at temperatures T and $T + \Delta T_s$ being far enough from $T_{N,\text{exp}}$. Then one gets $\Delta\phi_d \propto L\Delta L$, and the expression Eq. (3) is reduced to a form

$$\begin{aligned}\Delta\phi_d(T) &= DL \frac{dL}{dT} \Delta T_s(T) \\ &= -2D\beta(T_N - T)^{2\beta-1} \Delta T_s(T).\end{aligned}\quad (4)$$

As readily seen from Eq. (4), demagnetization time τ_2 correlates with the time required for the heating of the spin subsystem τ_s . The temperature evolution of $\Delta\phi_d$, in turn, depends on both β and the heating of the spin system. To analyze the response of the spins to optical excitation we employ a two-temperature model [53], considering that in laser-driven dielectrics energy and angular momentum transfer to spins is realized from the phonon subsystem [for a review, see Ref. [54]] and, thus, it is sufficient to consider only these two reservoirs with effective temperatures T_s and T_p , given the electron-phonon relaxation is fast and is of order of 2 ps (see Appendix for details). Here we assume that the energy delivered by the pump pulse is absorbed by electrons through $d-d$ and charge-transfer transitions and rapidly deposited to the lattice.

We solve the following system of equations with the initial condition $T_p = T_s = T$:

$$\begin{aligned}\frac{\rho}{\mu} C_p(T_p) \frac{dT_p}{dt} &= g_{sp}(T_s - T_p) + P(t), \\ \frac{\rho}{\mu} C_s(T_s) \frac{dT_s}{dt} &= g_{sp}(T_p - T_s),\end{aligned}\quad (5)$$

where C_p and C_s are lattice and magnetic molar specific heat, respectively, and g_{sp} is the spin-lattice coupling constant. $C_p(T)$ was determined by an approximation of experimental data on the total specific heat $C(T)$ reported in Ref. [42] with the Debye function [55]. Magnetic heat capacity was then obtained as $C_s(T) = C(T) - C_p(T)$. ρ and μ are the density and the molar mass, respectively. $P(t)$ is the absorbed laser power density found for the flake with a thickness $d \approx 200$ nm as [56]

$$P(t) = AF \frac{(1 - e^{-\alpha d})}{d} \frac{2\sqrt{\ln 2} e^{-4 \ln 2 t^2/\sigma^2}}{\sigma\sqrt{\pi}},\quad (6)$$

where A and α are absorbance and absorption coefficient, respectively. Absorbance $A = 1 - R$ was calculated using the Fresnel formula for reflection R at the air-MPS₃ interface with a complex refractive index n . Contributions from the reflections at other interfaces do not exceed 10% and are not taken into account. Other parameters used in calculations are presented in Table I.

Solving Eq. (5), we find both the temporal evolution of the spin temperature $\Delta T_s(\Delta t)$ and the heating of the spin system ΔT_s at time delay Δt_d . In NiPS₃ and FePS₃ the increase in the spin temperature ΔT_s is below 20 and 10 K, respectively, and has a minimum in the vicinity of $T_{N,\text{exp}}$. This justifies a direct comparison of the characteristic time of the spin temperature increase τ_s and the demagnetization time τ_2 according to the linearized expression [Eq. (4)]. By fitting $\Delta T_s(\Delta t)$ with a function $1 - e^{-\Delta t/\tau_s(T)}$, we obtain τ_s and compare it with the demagnetization time τ_2 at different initial temperatures. Note that the fitting procedure also involved correction for

TABLE I. Material parameters used in calculations, spin-phonon coupling constant g_{sp} and critical exponent β obtained from the fit for NiPS₃ and FePS₃.

Parameter	NiPS ₃	FePS ₃
ρ (kg m ⁻³)	3200 [57]	2900 [57]
μ (kg mol ⁻¹)	0.186	0.183
n	$3.7 + 0.5i$ [58]	$2.9 + 0.3i$ [59]
α (m ⁻¹)	3.2×10^6 [60]	1.2×10^6 [36,61]
g_{sp} (Wm ⁻³ K ⁻¹)	$(3.2 \pm 0.8) \times 10^{16a}$	$(1.2 \pm 0.4) \times 10^{16a}$
β	0.21 ± 0.06^a	0.10 ± 0.03^a

^aThis work.

$T_{N,\text{exp}} < T_N$ due to unideal thermal contact in the cryostat and excess laser heating. It was found to be ≈ 13 K in both samples, which yielded $T_{N,\text{exp}} = 142$ K for NiPS₃ and $T_{N,\text{exp}} = 105$ K for FePS₃. Since τ_s is essentially the spin-lattice thermalization time and is determined by the spin-lattice coupling constant g_{sp} , this allows us to find values of g_{sp} . Figures 3(c) and 4(b) show the calculated thermalization time $\tau_s(T)$ plotted along with τ_2 for NiPS₃ and FePS₃, respectively. Reasonable agreement with the experimentally obtained temperature dependence of the demagnetization time is obtained for both compounds at the values of g_{sp} listed in Table I.

As a next step, we fitted the temperature dependence of $\Delta\phi_d(T)$ below $T_{N,\text{exp}}$ with the function [Eq. (3)] using scaling coefficient D and critical exponent β as parameters [see solid green lines in Figs. 3(a) and 4(a)]. We obtained $\beta = 0.21 \pm 0.06$ for NiPS₃ close to the values 0.231 corresponding to the 2D XY model [44,62] and 0.24 ± 0.04 obtained from the temperature-dependent Raman scattering lines [inset in Fig. 1(e)]. For FePS₃, the critical exponent amounts to $\beta = 0.10 \pm 0.03$ in agreement with the 2D Ising model ($\beta = 0.125$ [44]) and data obtained from Mössbauer measurements ($\beta = 0.16 \pm 0.01$ [63]).

We note that in a range of ≈ 10 K above $T_{N,\text{exp}}$, there is still a weak nonzero transient exLD signal whose time constant τ_2 follows the spin temperature rise time τ_s [see Figs. 3(c) and 4(b)]. This signal can originate from the presence of short-range magnetic ordering, which is not accounted for in the model, and, thus, the amplitude of the transient exLD in this range is not described by Eq. (3) [see Figs. 3(a) and 4(a)].

IV. DISCUSSION

The performed analysis accounting for the laser-induced heating and spin-phonon coupling captures the main experimental finding. Transient exLD indeed measures the demagnetization due to laser-induced heating and is governed by the increase in spin temperature. Because of the thermal nature of the laser-induced changes, transient exLD and demagnetization ΔL itself possess critical behavior at T_N defined by the critical exponent β . Criticality agrees well with the one predicted by 2D XY or 2D Ising models.

The demagnetization characteristic time is, in turn, defined by the spin-lattice coupling constant g_{sp} and the temperature dependence of the spin specific heat, $\tau_2 = \tau_s = C_s/g_{sp}$. Pronounced slowing down of the demagnetization near the Néel temperature observed in FePS₃ is in agreement with previous

works. In contrast, it is negligible in NiPS₃. This correlates well with the features of the specific heat in these materials reported earlier in [25,42,64]. The heat capacity of NiPS₃ does not have a well-pronounced feature at T_N , while that of FePS₃ demonstrates a pronounced λ peak in $C_s(T)$.

We note that the difference in the critical behavior of demagnetization times in NiPS₃ and FePS₃ resembles the recently reported critical behavior of characteristic times of restoration of the equilibrium magnetic ordering [29]. These times are much longer than the demagnetization times and can be associated with the low interplanar thermal conductivity [65] governing the cooling down process. In the vicinity of T_N in FePS₃, this time shows a pronounced slowing down, reaching 1000 ps, and appears to be two orders of magnitude longer than in NiPS₃.

Spin-phonon coupling constants g_{sp} are found to be of the same order of magnitude for NiPS₃ and FePS₃, see Table I. This, in particular, stems from comparable demagnetization times of around 10 ps in these compounds, apart from the temperature range in the vicinity of T_N . Note that in Ref. [32], similar demagnetization time was reported for FePS₃ in a bulk limit. As for the other two MPS₃ compounds, MnPS₃ and CoPS₃, the demagnetization times well below the corresponding T_N were reported to be 30 ps [66] and 2 ps [30], respectively. Adding our data for NiPS₃ and FePS₃ to this set reveals that the demagnetization time below T_N in the MPS₃ family decreases in the row Mn–Fe, Ni–Co. One notes that this trend does not have a direct correlation with the trend in the Néel temperatures, since NiPS₃ has the highest T_N , FePS₃ and CoPS₃ have very close T_N [67], while the T_N for MnPS₃ is as low as 78 K [50]. Also, there is no direct correlation with the magnitudes of magnetic moments in these compounds either [50]. This is in contrast to demagnetization in metals [6]. We could speculate that in MPS₃, unquenching of orbital momentum, the most present in CoPS₃ and absent in MnPS₃, affects spin-phonon coupling and, thus, demagnetization times.

To address dependences of the demagnetization degree and time on pump photon energy, we note that they demonstrate no features, apart from the local maximum in $\Delta\phi_d$ at $E_p = 1.88$ eV in NiPS₃ [Fig. 3(b)]. Demagnetization time does not show any pronounced trend within the precision of our experiments [Fig. 3(d)]. On the other hand, in the studied spectral range, optical absorption steadily grows with photon energy due to increased contribution from charge-transfer transitions [36], resulting in an increase of the absorbed pump power. If the initial temperature is far enough below T_N , an increase in absorbed laser power P should lead to a slowdown of demagnetization by $\approx 20\%$ with a concomitant increase in its amplitude, as can be shown based on Eqs. (3) and (5). Such a slowing down cannot be resolved in our experiments [Figs. 3(c) and 3(d)]. We note, however, that the demagnetization degree in NiPS₃ appears to be sensitive to the localized d - d transition at $E_p = 1.88$ eV in NiPS₃ [49,50]. This may indicate that there can be an efficient channel of energy dissipation from electrons excited to $3d$ sublevels of Ni²⁺ to phonons involved in spin-phonon coupling g_{sp} . These can be, e.g., shear phonons, whose particular role in demagnetization was revealed recently [29]. Noticeably, no resonant enhancement is found in FePS₃, and there are no reports in

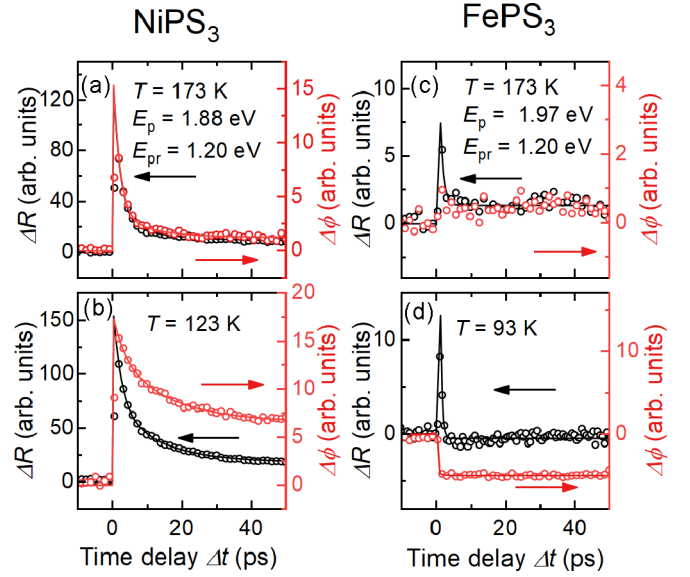


FIG. 5. Comparison of raw experimental traces for laser-induced probe polarization rotation $\Delta\phi(\Delta t)$ (red) and laser-induced change of reflectivity $\Delta R(\Delta t)$ (black) measured in NiPS₃ at (a) $T = 173$ K $> T_N$ and (b) $T = 123$ K $< T_N$, and in FePS₃ at (c) $T = 173$ K $> T_N$ and (d) $T = 93$ K $< T_N$. Solid lines are guides for the eye.

the literature on any pronounced features in the absorption spectrum of this material in the studied spectral range. This can be due to a narrower band gap in FePS₃ as compared to NiPS₃ (1.5 vs. 1.7 eV [36]), and, thus, a less pronounced contribution to absorption from d - d transitions. These observations, however, require further studies.

Finally, we discuss possible reasons for the transient decrease of exLD with the characteristic time τ_1 observed in FePS₃. Temperature dependences $\Delta\phi(\Delta t = 2$ ps) and τ_1 [Figs. 4(a) and 4(b)] suggest that the increase in spin temperature and the corresponding decrease of \mathbf{L} cannot be responsible for this signal, as discussed in Sec. III A. On the other hand, in optical pump-probe measurements, changes in the measured signal may also be caused by the laser-induced changes of the proportionality coefficient D between the polarization rotation and the magnetic characteristic [68], that is $\Delta\phi \propto \Delta D L^2$. Such a contribution to $\Delta\phi$ would follow the temperature dependence of static exLD ϕ and decrease in the vicinity of $T_{N,exp}$, as we observed in the experiment [Fig. 4(a)]. In the case of exLD, D includes optical parameters as well as the exchange coupling J . Measurements of the laser-induced dynamics of reflectivity $\Delta R(\Delta t)$ in FePS₃ revealed that it is characterized by a fast drop with a time constant of 1.5 ps (see Appendix and Fig. 5), which is close to τ_1 .

Thus, it is reasonable to assume that the faster dynamics of exLD is a trivial result of changes in optical properties leading to ΔD . Alternatively, the faster contribution to $\Delta\phi$ may stem from laser-induced perturbation of J due to rapid energy transfer to phonons, which, in general, can modulate Fe²⁺-S¹⁻ bonds responsible for exchange coupling. A fast change of ΔR can serve as a measure of this energy transfer rate. The feasibility of such phonon-modulated exchange and related transient magneto-optical response was investigated in Ref. [11] for the case of a dielectric ferrimagnet Y₃Fe₅O₁₂

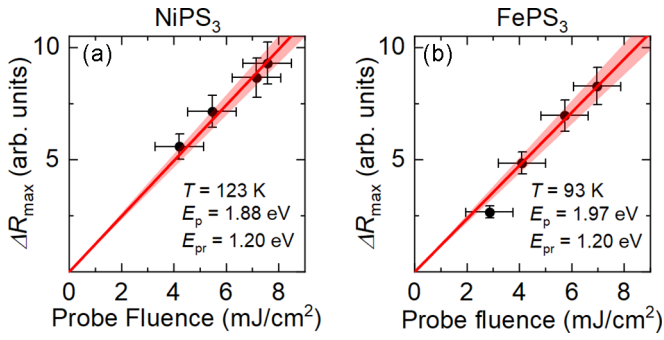


FIG. 6. Magnitude of laser-induced change of reflectivity ΔR as a function of probe pulse fluence (symbols) for (a) NiPS₃ at $T = 123$ K $< T_N$, and (b) FePS₃ at $T = 93$ K $< T_N$. The red solid line shows a linear fit with a confidence interval.

subjected to THz pump pulses. We also note that the magnitude of ΔR was found to gradually increase as the temperature was changed across $T_{N,exp}$ towards lower temperatures, which may point to the sensitivity of the electron-phonon coupling to the magnetic ordering.

V. CONCLUSIONS

A comparative experimental study of the laser-induced exLD in 2D zigzag antiferromagnets NiPS₃ and FePS₃ with XY- and Ising-like magnetic ordering revealed that ultrafast demagnetization in these compounds can be well understood in terms of laser-induced heating of the spin system mediated by spin-phonon coupling. The demagnetization degree shows critical behavior as Néel temperature is approached, with exponents being in good agreement with 2D XY- and 2D Ising-like ordering in NiPS₃ and FePS₃, respectively. The spin-phonon coupling parameter is found to be close for two compounds. Similarly, the demagnetization times well below T_N appear to be close and are of the order of 10 ps. Previously, demagnetization times were reported for all antiferromagnets from the MPS₃ family except for NiPS₃. Our data complete this row and show that the time decreases with a change of transition-metal Mn–Fe,Ni–Co. This highlights that unquenched orbital momentum, which is the strongest in Co²⁺ and is absent in Mn²⁺, plays an important role in ultrafast demagnetization in MPS₃. Apart from similarities, a difference in demagnetization times in NiPS₃ and FePS₃ was found in the vicinity of their respective T_N . The critical slowdown is observed in FePS₃ only and is nearly absent in NiPS₃. In agreement with the thermal nature of the laser-induced demagnetization, this difference is found to be related to the different behavior of spin specific heat in the vicinity of T_N .

ACKNOWLEDGMENTS

We thank R. M. Dubrovin for the help with experiments. We thank D. Bossini for insightful discussions. The work of D.V.K., V.Yu.D., and A.M.K. was supported by Russian Foundation for Basic Research Grant No. 19-52-12065. M.A.P. acknowledges support of Russian Science Foundation under Grant No. 22-72-00039. L.A.Sh. acknowledges Presidential Scholarship Grant No. SP-4623.2022.5. M.C. and F.M. acknowledge support by the Deutsche Forschungsgemeinschaft through the International Collaborative Research Centre 160 (Projects B9 and Z4). E.C. and M.C. acknowledge funding from the European Union’s Horizon 2020 Research and Innovation Programme under Project SINFORIA, Grant No. 964396. E.C. acknowledges support from the European Union (ERC-2017-ADG-788222), from the Spanish Government (2D-HETEROS PID2020-117152RB-I00, co-financed by FEDER, and Excellence Unit “María de Maeztu” CEX2019-000919-M) and the Generalitat Valenciana (PROMETEO Program and PO FEDER Program, IDIFEDER/2018/061). E.C. acknowledges the Advanced Materials program, supported by MCIN with funding from European Union NextGenerationEU (PRTR-C17.I1) and by Generalitat Valenciana.

APPENDIX: LASER-INDUCED REFLECTIVITY DYNAMICS

In Fig. 5, we present the raw signals $\Delta\phi(\Delta t)$ and $\Delta R(\Delta t)$ in NiPS₃ and FePS₃ at temperatures above and below T_N . The dynamics of the reflectivity change is characterized by the time constant amounting to 2 ps in NiPS₃ and 1.5 ps in FePS₃, which is related to the electron-phonon relaxation time and depends on temperature only weakly.

In both compounds at $T > T_N$, $\Delta\phi(\Delta t)$ and $\Delta R(\Delta t)$ show similar dynamics [Figs. 5(a) and 5(c)]. Thus, we associate transient probe polarization rotation at these temperatures with the changes in the Fresnel coefficients of the flakes, as well as laser-induced changes in the substrate optical constants, strain-induced effects, etc.

At $T < T_N$, transients $\Delta\phi(\Delta t)$ and $\Delta R(\Delta t)$ show distinct behavior [Figs. 5(b) and 5(d)]. In particular, probe polarization rotation possesses an additional slower contribution as compared to the dynamics of reflectivity. This is the contribution from transient exLD, which can be obtained by subtraction of $\Delta\phi(\Delta t)$ measured at $T = 173$ K from the data measured below T_N , as discussed in the main text.

In order to verify that the measurements of the laser-induced dynamics are performed in the linear regime, we have measured pump-induced changes in reflectivity ΔR at different probe fluences. As shown in Fig. 6, there is a linear dependence of ΔR magnitude measured at $\Delta t = 2$ ps on the probe fluence in both FePS₃ and NiPS₃ samples.

[1] C. D. Stanciu, F. Hansteen, A. V. Kimel, A. Kirilyuk, A. Tsukamoto, A. Itoh, and T. Rasing, All-optical magnetic recording with circularly polarized light, *Phys. Rev. Lett.* **99**, 047601 (2007).

[2] T. A. Ostler, J. Barker, R. F. L. Evans, R. W. Chantrell, U. Atxitia, O. Chubykalo-Fesenko, S. El Moussaoui, L. Le Guyader, E. Mengotti, L. J. Heyderman, F. Nolting, A. Tsukamoto, A. Itoh, D. Afanasiev, B. A. Ivanov, A. M.

- Kalashnikova, K. Vahaplar, J. Mentink, A. Kirilyuk, T. Rasing *et al.*, Ultrafast heating as a sufficient stimulus for magnetization reversal in a ferrimagnet, *Nature Commun.* **3**, 666 (2012).
- [3] R. Medapalli, D. Afanasiev, D. K. Kim, Y. Quessab, S. Manna, S. A. Montoya, A. Kirilyuk, T. Rasing, A. V. Kimel, and E. E. Fullerton, Multiscale dynamics of helicity-dependent all-optical magnetization reversal in ferromagnetic Co/Pt multilayers, *Phys. Rev. B* **96**, 224421 (2017).
- [4] T. J. Huisman, R. V. Mikhaylovskiy, J. D. Costa, F. Freimuth, E. Paz, J. Ventura, P. P. Freitas, S. Blügel, Y. Mokrousov, T. Rasing, and A. V. Kimel, Femtosecond control of electric currents in metallic ferromagnetic heterostructures, *Nature Nanotechnol.* **11**, 455 (2016).
- [5] T. Seifert, S. Jaiswal, U. Martens, J. Hannegan, L. Braun, P. Maldonado, F. Freimuth, A. Kronenberg, J. Henrizi, I. Radu, E. Beaupaire, Y. Mokrousov, P. M. Oppeneer, M. Jourdan, G. Jakob, D. Turchinovich, L. M. Hayden, M. Wolf, M. Münzenberg, M. Kläui *et al.*, Efficient metallic spintronic emitters of ultrabroadband terahertz radiation, *Nature Photon.* **10**, 483 (2016).
- [6] B. Koopmans, G. Malinowski, F. D. Longa, D. Steiauf, M. Fähnle, T. Roth, M. Cinchetti, and M. Aeschlimann, Explaining the paradoxical diversity of ultrafast laser-induced demagnetization, *Nature Mater.* **9**, 259 (2010).
- [7] E. Beaupaire, J.-C. Merle, A. Daunois, and J.-Y. Bigot, Ultrafast spin dynamics in ferromagnetic nickel, *Phys. Rev. Lett.* **76**, 4250 (1996).
- [8] C. Stamm, T. Kachel, N. Pontius, R. Mitzner, T. Quast, K. Holldack, S. Khan, C. Lupulescu, E. F. Aziz, M. Wietstruk, H. A. Dürr, and W. Eberhardt, Femtosecond modification of electron localization and transfer of angular momentum in nickel, *Nature Mater.* **6**, 740 (2007).
- [9] E. Carpena, E. Mancini, C. Dallera, M. Brenna, E. Puppini, and S. De Silvestri, Dynamics of electron-magnon interaction and ultrafast demagnetization in thin iron films, *Phys. Rev. B* **78**, 174422 (2008).
- [10] A. V. Kimel, R. V. Pisarev, J. Hohlfeld, and T. Rasing, Ultrafast quenching of the antiferromagnetic order in FeBO₃: Direct optical probing of the phonon-magnon coupling, *Phys. Rev. Lett.* **89**, 287401 (2002).
- [11] S. F. Maehrlein, I. Radu, P. Maldonado, A. Paarmann, M. Gensch, A. M. Kalashnikova, R. V. Pisarev, M. Wolf, P. M. Oppeneer, J. Barker, and T. Kampfrath, Dissecting spin-phonon equilibration in ferrimagnetic insulators by ultrafast lattice excitation, *Sci. Adv.* **4**, eaar5164 (2018).
- [12] V. López-Flores, N. Bergeard, V. Halté, C. Stamm, N. Pontius, M. Hehn, E. Otero, E. Beaupaire, and C. Boeglin, Role of critical spin fluctuations in ultrafast demagnetization of transition-metal rare-earth alloys, *Phys. Rev. B* **87**, 214412 (2013).
- [13] J. Kimling, J. Kimling, R. B. Wilson, B. Hebler, M. Albrecht, and D. G. Cahill, Ultrafast demagnetization of FePt:Cu thin films and the role of magnetic heat capacity, *Phys. Rev. B* **90**, 224408 (2014).
- [14] M. A. Susner, M. Chyashvichyus, M. A. McGuire, P. Ganesh, and P. Maksymovych, Metal thio- and selenophosphates as multifunctional van der Waals layered materials, *Adv. Mater.* **29**, 1602852 (2017).
- [15] F. Wang, T. A. Shifa, P. Yu, P. He, Y. Liu, F. Wang, Z. Wang, X. Zhan, X. Lou, F. Xia, and J. He, New frontiers on van der Waals layered metal phosphorous trichalcogenides, *Adv. Funct. Mater.* **28**, 1802151 (2018).
- [16] C. Bellitto, E. M. Bauer, and G. Righini, Organic-inorganic hybrids: From magnetic perovskite metal(II) halides to multifunctional metal(II) phosphonates, *Coord. Chem. Rev.* **289–290**, 123 (2015).
- [17] A. S. Ingason, M. Dahlqvist, and J. Rosen, Magnetic MAX phases from theory and experiments; a review, *J. Phys.: Condens. Matter* **28**, 433003 (2016).
- [18] S. Jenkins, L. Rózsa, U. Atxitia, R. F. L. Evans, K. S. Novoselov, and E. J. G. Santos, Breaking through the Mermin-Wagner limit in 2D van der Waals magnets, *Nature Commun.* **13**, 6917 (2022).
- [19] C.-T. Kuo, M. Neumann, K. Balamurugan, H. J. Park, S. Kang, H. W. Shiu, J. H. Kang, B. H. Hong, M. Han, T. W. Noh *et al.*, Exfoliation and Raman spectroscopic fingerprint of few-layer NiPS₃ van der Waals crystals, *Sci. Rep.* **6**, 20904 (2016).
- [20] M. Xu, T. Liang, M. Shi, and H. Chen, Graphene-like two-dimensional materials, *Chem. Rev.* **113**, 3766 (2013).
- [21] R. Mas-Ballesté, C. Gómez-Navarro, J. Gómez-Herrero, and F. Zamora, 2D materials: to graphene and beyond, *Nanoscale* **3**, 20 (2011).
- [22] S. Z. Butler, S. M. Hollen, L. Cao, Y. Cui, J. A. Gupta, H. R. Gutiérrez, T. F. Heinz, S. S. Hong, J. Huang, A. F. Ismach, E. Johnston-Halperin, M. Kuno, V. V. Plashnitsa, R. D. Robinson, R. S. Ruoff, S. Salahuddin, J. Shan, L. Shi, M. G. Spencer, M. Terrones *et al.*, Progress, challenges, and opportunities in two-dimensional materials beyond graphene, *ACS Nano* **7**, 2898 (2013).
- [23] B. Huang, G. Clark, E. Navarro-Moratalla, D. R. Klein, R. Cheng, K. L. Seyler, D. Zhong, E. Schmidgall, M. A. McGuire, D. H. Cobden, W. Yao, D. Xiao, P. Jarillo-Herrero, and X. Xu, Layer-dependent ferromagnetism in a van der Waals crystal down to the monolayer limit, *Nature (London)* **546**, 270 (2017).
- [24] K. Kim, S. Y. Lim, and J. U. Lee, Suppression of magnetic ordering in XXZ-type antiferromagnetic monolayer NiPS₃, *Nature Commun.* **10**, 08284 (2019).
- [25] T. Y. Kim and C.-H. Park, Magnetic anisotropy and magnetic ordering of transition-metal phosphorus trisulfides, *Nano Lett.* **21**, 10114 (2021).
- [26] A. Caretta, M. C. Donker, A. O. Polyakov, T. T. M. Palstra, and P. H. M. van Loosdrecht, Photoinduced magnetization enhancement in two-dimensional weakly anisotropic Heisenberg magnets, *Phys. Rev. B* **91**, 020405(R) (2015).
- [27] F. Mertens, D. Mänkebüscher, U. Parlak, C. Boix-Constant, S. Mañas-Valero, M. Matzer, R. Adhikari, A. Bonanni, E. Coronado, A. M. Kalashnikova, D. Bossini, and M. Cinchetti, Ultrafast coherent THz lattice dynamics coupled to spins in the van der Waals antiferromagnet FePS₃, *Adv. Mater.* **35**, 2208355 (2023).
- [28] D. Afanasiev, J. R. Hortensius, M. Matthesen, S. Mañas-Valero, M. Šiškins, M. Lee, E. Lesne, H. S. J. van der Zant, P. G. Steeneken, B. A. Ivanov, E. Coronado, and A. D. Caviglia, Controlling the anisotropy of a van der Waals antiferromagnet with light, *Sci. Adv.* **7**, eabf3096 (2021).
- [29] F. Zhou, K. Hwangbo, Q. Zhang, C. Wang, L. Shen, J. Zhang, Q. Jiang, A. Zong, Y. Su, M. Zajac, Y. Ahn, D. A. Walko, R. D. Schaller, J.-H. Chu, N. Gedik, X. Xu, D. Xiao, and H. Wen, Dynamical criticality of spin-shear coupling in van der Waals antiferromagnets, *Nature Commun.* **13**, 6598 (2022).

- [30] D. Khusyainov, T. Gareev, V. Radovskaia, K. Sampathkumar, S. Acharya, M. Šiškins, S. Mañas-Valero, B. A. Ivanov, E. Coronado, T. Rasing, A. V. Kimel, and D. Afanasiev, Ultrafast laser-induced spin-lattice dynamics in the van der Waals antiferromagnet CoPS_3 , *APL Mater.* **11**, 071104 (2023).
- [31] T. Lichtenberg, C. F. Schippers, S. C. P. van Kooten, S. G. F. Evers, B. Barcones, M. H. D. Guimarães, and B. Koopmans, Anisotropic laser-pulse-induced magnetization dynamics in van der Waals magnet Fe_3GeTe_2 , *2D Mater.* **10**, 015008 (2023).
- [32] X.-X. Zhang, S. Jiang, J. Lee, C. Lee, K. F. Mak, and J. Shan, Spin dynamics slowdown near the antiferromagnetic critical point in atomically thin FePS_3 , *Nano Lett.* **21**, 5045 (2021).
- [33] G. Ouvrard, R. Brec, and J. Rouxel, Structural determination of some MPS_3 layered phases ($M = \text{Mn, Fe, Co, Ni}$ and Cd), *Mater. Res. Bull.* **20**, 1181 (1985).
- [34] P. A. Joy and S. Vasudevan, Magnetism in the layered transition-metal thiophosphates MPS_3 ($M = \text{Mn, Fe, Ni}$), *Phys. Rev. B* **46**, 5425 (1992).
- [35] A. R. Wildes, V. Simonet, E. Ressouche, G. J. McIntyre, M. Avdeev, E. Suard, S. A. J. Kimber, D. Lançon, G. Pepe, B. Moubaraki, and T. J. Hicks, Magnetic structure of the quasi-two-dimensional antiferromagnet NiPS_3 , *Phys. Rev. B* **92**, 224408 (2015).
- [36] R. Brec, D. M. Schleich, G. Ouvrard, A. Louisy, and J. Rouxel, Physical properties of lithium intercalation compounds of the layered transition chalcogenophosphates, *Inorg. Chem.* **18**, 1814 (1979).
- [37] V. Grasso, S. Santangelo, and M. Piacentini, Optical absorption spectra of some transition metal thiophosphates, *Solid State Ionics* **20**, 9 (1986).
- [38] D. S. Kim, D. Huang, C. Guo, K. Li, D. Rocca, F. Y. Gao, J. Choe, D. Lujan, T. Wu, K. Lin, E. Baldini, L. Yang, S. Sharma, R. Kalaivanan, R. Sankar, S. Lee, Y. Ping, and X. Li, Anisotropic excitons reveal local spin chain directions in a van der Waals antiferromagnet, *Adv. Mater.* **35**, 2206585 (2023).
- [39] D. Lançon, H. C. Walker, E. Ressouche, B. Ouladdiaf, K. C. Rule, G. J. McIntyre, T. J. Hicks, H. M. Rønnow, and A. R. Wildes, Magnetic structure and magnon dynamics of the quasi-two-dimensional antiferromagnet FePS_3 , *Phys. Rev. B* **94**, 214407 (2016).
- [40] J.-U. Lee, S. Lee, J. H. Ryoo, S. Kang, T. Y. Kim, P. Kim, C.-H. Park, J.-G. Park, and H. Cheong, Ising-type magnetic ordering in atomically thin FePS_3 , *Nano Lett.* **16**, 7433 (2016).
- [41] K. Momma and F. Izumi, *VESTA3* for three-dimensional visualization of crystal, volumetric and morphology data, *J. Appl. Crystallogr.* **44**, 1272 (2011).
- [42] M. Šiškins, M. Lee, S. Mañas-Valero, E. Coronado, Y. M. Blanter, H. S. van der Zant, and P. G. Steeneken, Magnetic and electronic phase transitions probed by nanomechanical resonators, *Nature Commun.* **11**, 16430 (2020).
- [43] S. Liu, A. Granados del Águila, D. Bhowmick, C. K. Gan, T. Thu Ha Do, M. A. Prosnikov, D. Sedmidubský, Z. Sofer, P. C. M. Christianen, P. Sengupta, and Q. Xiong, Direct observation of magnon-phonon strong coupling in two-dimensional antiferromagnet at high magnetic fields, *Phys. Rev. Lett.* **127**, 097401 (2021).
- [44] C. A. Vaz, J. A. Bland, and G. Lauhoff, Magnetism in ultrathin film structures, *Rep. Prog. Phys.* **71**, 056501 (2008).
- [45] X. Wang, K. Du, Y. Y. F. Liu, P. Hu, J. Zhang, Q. Zhang, M. H. S. Owen, X. Lu, C. K. Gan, P. Sengupta, C. Kloc, and Q. Xiong, Raman spectroscopy of atomically thin two-dimensional magnetic iron phosphorus trisulfide (FePS_3) crystals, *2D Mater.* **3**, 031009 (2016).
- [46] Q. Zhang, K. Hwangbo, C. Wang, Q. Jiang, J.-H. Chu, H. Wen, D. Xiao, and X. Xu, Observation of giant optical linear dichroism in a zigzag antiferromagnet FePS_3 , *Nano Lett.* **21**, 6938 (2021).
- [47] P. Markovin and R. Pisarev, Magnetic, thermal, and elastic refraction of light in the antiferromagnet MnF_2 , *ZhETF* **77**, 2461 (1979) [*Sov. Phys. JETP* **50**, 1190 (1979)].
- [48] V. Saidl, P. Němec, P. Wadley, V. Hills, R. P. Campion, V. Novák, K. W. Edmonds, F. Maccherozzi, S. S. Dhesi, B. L. Gallagher, F. Trojánek, J. Kuneš, J. Železný, P. Malý, and T. Jungwirth, Optical determination of the Néel vector in a CuMnAs thin-film antiferromagnet, *Nature Photon.* **11**, 91 (2017).
- [49] E. J. K. B. Banda, Optical absorption of NiPS_3 in the near-infrared, visible and near-ultraviolet regions, *J. Phys. C* **19**, 7329 (1986).
- [50] P. A. Joy and S. Vasudevan, Optical-absorption spectra of the layered transition-metal thiophosphates MPS_3 ($M = \text{Mn, Fe, Ni}$), *Phys. Rev. B* **46**, 5134 (1992).
- [51] S. O. Demokritov, N. M. Kreines, and V. I. Kudinov, Inelastic scattering of light in the antiferromagnet EuTe , *ZhETF* **92**, 689 (1987) [*Sov. Phys. JETP* **65**, 389 (1987)].
- [52] L. Landau and E. Lifshitz, Phase transitions of the second kind and critical phenomena, in *Statistical Physics*, 3rd ed., edited by L. Landau and E. Lifshitz (Butterworth-Heinemann, Oxford, 1980), Chap. XIV, pp. 446–516.
- [53] S. Anisimov, B. Kapeliovich, and T. Perelman, Electron emission from metal surfaces exposed to ultrashort laser pulses, *ZhETF* **66**, 776 (1974) [*Sov. Phys. JETP* **39**, 375 (1974)].
- [54] A. Kirilyuk, A. V. Kimel, and T. Rasing, Ultrafast optical manipulation of magnetic order, *Rev. Mod. Phys.* **82**, 2731 (2010).
- [55] P. Debye, Zur Theorie der spezifischen Wärmen, *Ann. Phys.* **344**, 789 (1912).
- [56] J. Walowski, Physics of laser heated ferromagnets: Ultrafast demagnetization and magneto-Seebeck effect, Ph.D. thesis, Georg-August-University Göttingen, 2012, <http://dx.doi.org/10.53846/goediss-2944>.
- [57] A. Jain, S. P. Ong, G. Hautier, W. Chen, W. D. Richards, S. Dacek, S. Cholia, D. Gunter, D. Skinner, G. Ceder, and K. A. Persson, Commentary: The materials project: A materials genome approach to accelerating materials innovation, *APL Mater.* **1**, 011002 (2013).
- [58] M. Piacentini, F. S. Khumalo, C. G. Olson, J. W. Andereg, and D. W. Lynch, Optical transitions, XPS, and electronic states in NiPS_3 , *Chem. Phys.* **65**, 289 (1982).
- [59] H. Zhang, Z. Ni, C. E. Stevens, A. Bai, F. Peiris, J. R. Hendrickson, L. Wu, and D. Jariwala, Cavity-enhanced linear dichroism in a van der Waals antiferromagnet, *Nature Photon.* **16**, 311 (2022).
- [60] C. A. Belvin, E. Baldini, I. O. Ozel, D. Mao, H. C. Po, C. J. Allington, S. Son, B. H. Kim, J. Kim, I. Hwang, J. H. Kim, J. G. Park, T. Senthil, and N. Gedik, Exciton-driven antiferromagnetic metal in a correlated van der Waals insulator, *Nature Commun.* **12**, 4837 (2021).

- [61] A. K. Budniak, S. J. Zelewski, M. Birowska, T. Woźniak, T. Bendikov, Y. Kauffmann, Y. Amouyal, R. Kudrawiec, and E. Lifshitz, Spectroscopy and structural investigation of iron phosphorus trisulfide FePS_3 , *Adv. Opt. Mater.* **10**, 2102489 (2022).
- [62] J. V. José, L. P. Kadanoff, S. Kirkpatrick, and D. R. Nelson, Renormalization, vortices, and symmetry-breaking perturbations in the two-dimensional planar model, *Phys. Rev. B* **16**, 1217 (1977).
- [63] D. Yao-Dong, W. Lin, Y. Ya-Xin, H. Yun, H. Hong-Bo, and X. Yuan-Fu, A Mössbauer study of the magnetic coupling in iron phosphorous trisulfides, *Chin. Phys.* **13**, 1652 (2004).
- [64] Y. Takano, N. Arai, A. Arai, Y. Takahashi, K. Takase, and K. Sekizawa, Magnetic properties and specific heat of MPS_3 ($M = \text{Mn}, \text{Fe}, \text{Zn}$), *J. Magn. Magn. Mater.* **272–276**, E593 (2004).
- [65] A. J. Minnich, Exploring the extremes of heat conduction in anisotropic materials, *Nanoscale Microscale Thermophys. Eng.* **20**, 1 (2016).
- [66] M. Matthiesen, J. R. Hortensius, S. Mañas-Valero, I. Kapon, D. Dumcenco, E. Giannini, M. Šiškins, B. A. Ivanov, H. S. J. van der Zant, E. Coronado, A. B. Kuzmenko, D. Afanasiev, and A. D. Caviglia, Controlling magnetism with light in a zero orbital angular momentum antiferromagnet, *Phys. Rev. Lett.* **130**, 076702 (2023).
- [67] A. R. Wildes, V. Simonet, E. Ressouche, R. Ballou, and G. J. McIntyre, The magnetic properties and structure of the quasi-two-dimensional antiferromagnet CoPS_3 , *J. Phys.: Condens. Matter* **29**, 455801 (2017).
- [68] B. Koopmans, M. van Kampen, J. T. Kohlhepp, and W. J. M. de Jonge, Ultrafast magneto-optics in nickel: Magnetism or optics? *Phys. Rev. Lett.* **85**, 844 (2000).